Supporting Information

Exceptionally Stable Cobalt Nanoclusters on Functionalized Graphene

Valeria Chesnyak, Srdjan Stavrić, Mirco Panighel, Daniele Povoledo, Simone del Puppo, Maria Peressi, Giovanni Comelli, Cristina Africh*

General aspects of the graphene quality (Related to experimental section in the main text)

Images of the different representative G layers can be found in S1 for rotated and aligned domains of each Ni surface orientation, together with corresponding LEED patterns. Rotated domains on Ni(100), visible in Figure S1 a, exhibit a stripy moiré misaligned with respect to the N(100) lattice vectors. Usually, they are found to be rich of incorporated Ni atoms. A G layer with the majority of such rotated domains can be obtained when the G growth is performed at 500 °C (corresponding LEED pattern shown in Figure S1 c). In turn, when the growth temperature is 560 °C, more aligned domains are formed, as shown in Figure S1 b. They are less likely to exhibit incorporated Ni atoms and the LEED pattern shows moiré spots close to the (00) aligned with the Ni(100) lattice vectors (encircled in white).

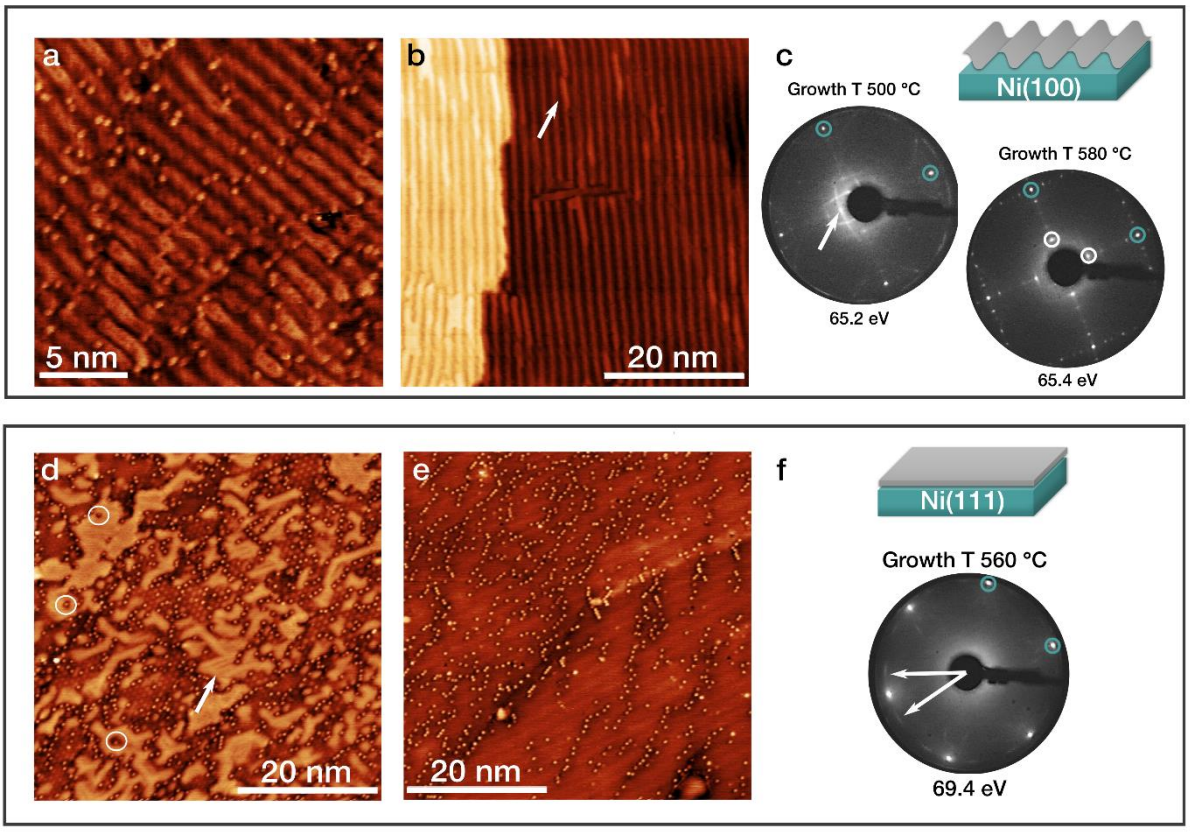

Figure S1. Different domains of G grown on Ni(100) exhibiting a large number of incorporated Ni atoms in (a) and almost none in (b). The growth temperature influences the predominant domain orientation visible in LEED, as shown in (c): at 500 °C mainly rotated domains are formed and the moiré-related spots (marked in white) close to (00) appear in lines, while at 560 °C more aligned domains are formed and the moiré-spots are aligned with the Ni(100) directions marked in turquoise. On Ni(111), epitaxial and aligned G is formed at 560 °C, (see panel (e)) and the LEED spots, visible in panel (f), coincide with the Ni(111) spots (encircled in turquoise), while the rotated domains (see image (d)) create elongated spots (marked in white). (a: I_t = 1.4 nA, V_b = -0.6 V, (b) I_t =0.9 nA, V_b =-0.6 V, (d) I_t =0.8 nA, V_b =-0.8 V, (e) I_t =0.8 nA, V_b =-0.8 V)

It is worth noting that some Ni-carbide (Ni_2C) formation, lifting the G into a quasi-free-standing state, typically occurs below the G layer on both Ni substrates at a temperature of 350 °C. Therefore, a fast cooling from 400 °C is applied and the absence of Ni_2C is confirmed by LEED: the carbide layer creates a (2 × 2) reconstruction which is normally not present in our case. However, small patches can be found, identified by a brighter appearance of the G layer, highlighted in Figure S1 b by a white arrow.

The G layer on Ni(111) follows the same behavior. Aligned domains, as depicted in Figure S1 e predominate when growing at 560 °C. The LEED pattern will show only the Ni(111) spots, as those of aligned G coincide. However, eventually some rotated domains can form too, like in Figure S1 d, yielding faint elongated spots in the LEED pattern in f. Besides the hexagonal moiré, the rotated regions exhibit some brighter islands, corresponding to the lifted G layer due to Ni_2C formation at the interface, just like in case of Ni(100). However, Ni_2C apparently emerges only below rotated domains on Ni(111) and does not lift the incorporated Ni atoms, so that they keep their binding to the substrate, as can be appreciated by the encircled Ni atoms that are surrounded by the Ni_2C patches. Both domains have a high density of Ni anchors, yet it is preferrable to obtain an aligned layer to prevent Ni_2C.

Analysis of cluster size

The size of clusters was estimated using the Gwyddion software. An intensity threshold masking tool is applied onto representative STM images to the clusters as shown in blue in Figure S2a. The extracted mask is shown in Figure S2b. The average radius of the grains and the height distribution of the selected clusters is shown in Figure S2, c and d, respectively. The mean radius has been evaluated by a gaussian fitting (red curve in c) and doubled to get the average diameter. For the average height, we took the value of the peak in the height distribution as shown in the graph in d with the vertical line. Maximum sizes were obtained by measuring selected larger clusters in the STM images.

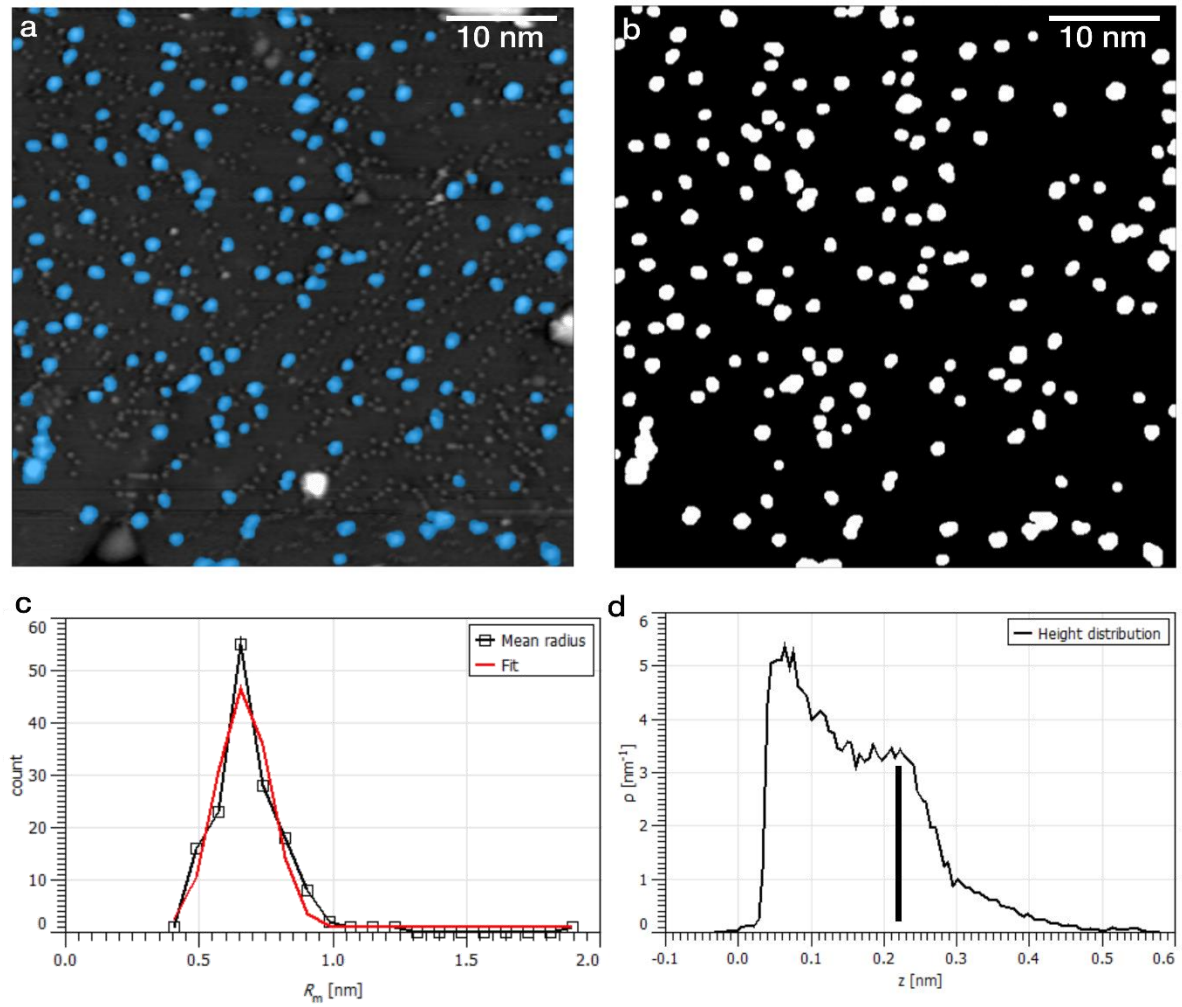

Figure S2. Cluster size analysis procedure. Clusters are selected in representative STM images using an intensity threshold mask as displayed in (a) with the corresponding extracted mask in (b). The average diameter of the clusters is given by a gaussian fit of the mean radius distributions of the mask grains (c). The average cluster height is extracted from the peak in the height distribution plot as shown by the vertical line in graph (d).

Higher Co loading and domain-dependent presence of clusters on Ni(100)

To understand if the small size of the clusters is due to the low coverage or to another feature provided by the support, the coverage was increased up to 0.21 ML, with a total evaporation time of 10 min + 1 h. To understand if the sample is behaving the same as in the previous preparations, we first acquired STM images after 10 min of evaporation to compare and after the additional hour of evaporation with the same parameters. The obtained clusters after the total evaporation are presented in Figure S3 a.

The cluster density has clearly increased, but no significant increase of the size is observed, as discussed in the main text.

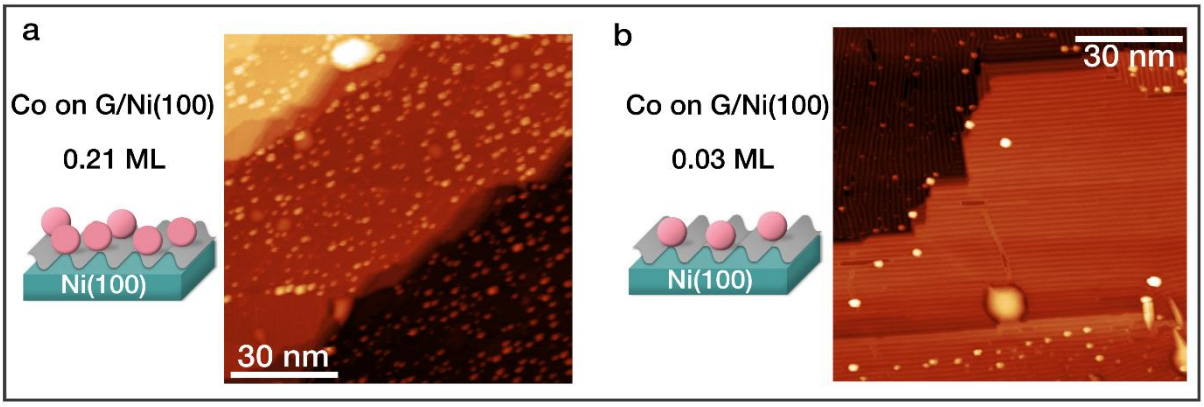

Figure S3. High Co loading on Ni(100) in (a) with 11 times higher coverage. Domain dependence of Co clusters on Ni(100) in (b), where the central high quality domain -lacking Ni anchors and thus with almost no Co clusters – is surrounded by anchor rich domains with normal cluster density. (a: I_t = 0.4 nA, V_b = -1.3 V, b: I_t = 0.8 nA, V_b = -0.8 V)

Still, there are some domains on Ni(100) which show lower Ni anchor concentration and thus lower cluster density, as depicted in Figure S3 b. Usually those domains appear well-defined, defect free and more aligned with the substrate, as in the center of the STM image in b); their abundance depends on the growth process. Perhaps due to the matching symmetry of aligned stacking, the G growth is happening faster as less strain occurs in this case. Therefore, there is less time for Ni incorporation and a high-quality domain is obtained. The domains around the center of Figure S3 b exhibit more defects and thus many adsorbed clusters.

DFT adsorption energy for multiatomic clusters

Figure S4 shows the adsorption energy calculated according to Equation (1) in the Main Text for Co clusters up to 4 atoms adsorbed on valleys and ridges on G/Ni(001), with and without the presence of a Ni adatoms trapped in a double vacancy in the G network. To simplify the picture, for each value of *n* only the result for the most stable structure is reported (see Figure 4 in the Main Text for the most stable structures).

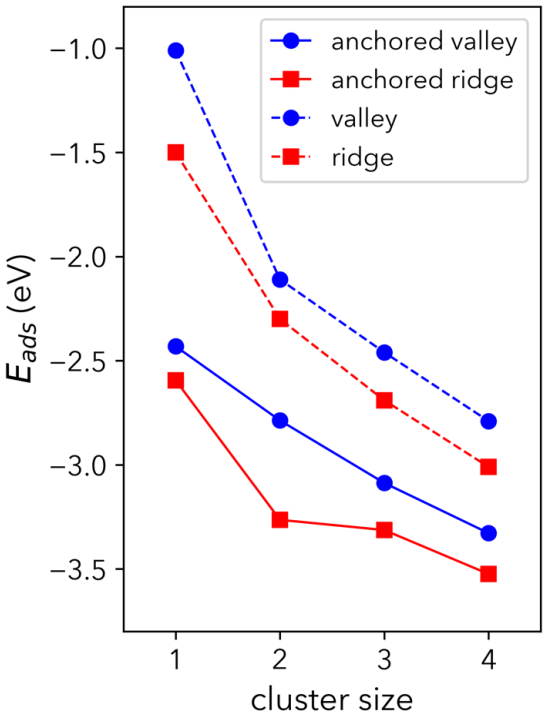

Figure S4. Calculated adsorption energy E_{ads} for Co_n clusters up to $n = 4$ atoms, on valleys (blue) and ridges (red) on G/Ni(001), with (solid lines) and without (dashed lines) anchoring.

CO dosage on Co/Ni(100)

Selected frames from the movie of the CO dosage, showing blinking events of the clusters, are presented in Figure S5. Green arrows indicate the individual clusters that change their contrast. Usually, in the subsequent frame they go back to their initial brightness, indicating a reversible adsorption process of CO on the Co clusters.

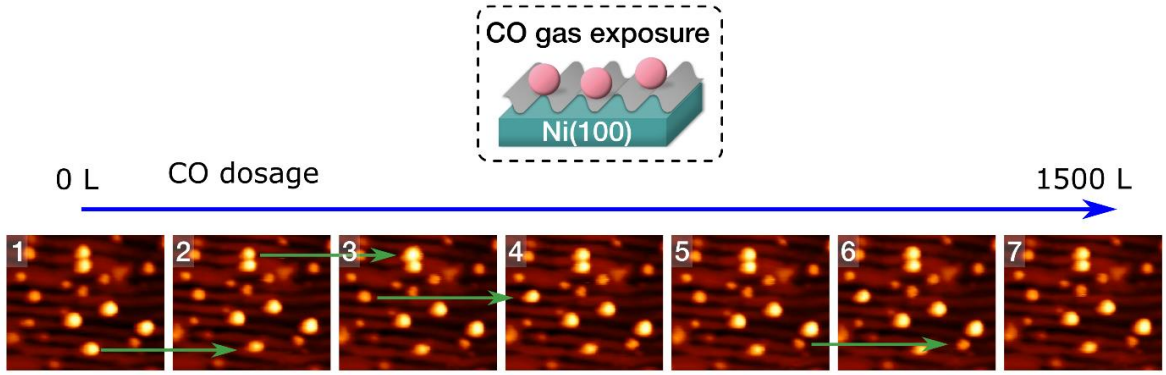

Figure S5. Individual frames extracted from the movie recorded during an overall CO dosage of 1500 L, showing blinking clusters highlighted by green arrows. (all: I_t = 0.3 nA, V_b = -1V, size: 16.8 × 14.5 nm^2)